GEOPHYSICS. VOL. 76, NO. 6 (NOVEMBER-DECEMBER 2011); P. WC5–WC15, 7 FIGS.
10.1190/GEO2011-0096.1

Earthquakes and errors: Methods for industrial applications

Gillian R. Foulger[1] and Bruce R. Julian[1]

ABSTRACT

The high accuracies and realistic confidence assessments demanded for seismic monitoring of hydraulic fracturing work require specialist experimental approaches. These include seismic network design based on quantitative modeling, high-quality instrument deployments, and accurate and detailed crustal models. Confidence estimates must take into account uncertainties about crustal structure, which may dominate error budgets. Earthquake size should be expressed in terms of scalar seismic moment or the associated moment magnitude M_W, which is related to fundamental physical source processes, and not as traditional earthquake magnitudes. Representing earthquake mechanisms in terms of seismic moment tensors allows for processes such as volume changes and complex types of shearing that are important in hydrocarbon and geothermal reservoirs. Traditional fault-plane solutions are based on simplifying assumptions such as shear slip on a planar faults, and isotropic crustal structures, which may introduce large uncertainties. Quantitative assessment of confidence regions for moment-tensor source mechanisms, a newly emerging field, is important for distinguishing computational artifacts from real physical phenomena. We review methods currently available for realistic error estimation for earthquake locations and moment tensors, with particular emphasis on surface sensor arrays in geothermal areas.

INTRODUCTION

The use of hydraulic fracturing as an aid to hydrocarbon extraction and for creating enhanced geothermal systems (EGS) is becoming increasingly widespread. Such operations often induce large numbers of small earthquakes (known as "microearthquakes," "microseismic events," or "fracking-induced events"). Like natural earthquakes, these events occur in response to rock failure and fluid motion. There is no evidence that they differ fundamentally in any way from naturally occurring earthquakes in geothermal and hydrocarbon reservoirs or, for that matter, other contexts, e.g., on tectonic faults. The techniques applicable to studying both industrially induced and naturally occurring earthquakes are thus fundamentally the same.

The sizes of earthquakes are fractally distributed, regardless of the context in which they occur. As a result, swarms of many small earthquakes are accompanied by the occasional larger event which is not technically a "microearthquake" (i.e., an earthquake that is not felt at the surface). For this reason, we use the terms "earthquake" or "event" in this paper. Hydraulic fracturing operations aim to manage the sizes of induced events so they do not cause ground shaking at the surface that is strong enough to be a societal nuisance.

Earthquake seismology ("passive seismology") has a history of technological development about a century long. During this time, methods have been developed to use recordings of earthquakes to calculate earth structure, hypocenter locations, magnitudes, and source mechanisms. For most of this time, work has primarily targeted academic and hazard-reduction objectives. Achieving these objectives does not necessarily require high levels of accuracy. For example, the exact locations of earthquakes at the level of a few meters are not critical for tectonic studies or hazard reduction. Likewise, although earthquake sizes and source mechanisms are required to inform those applications, extreme levels of accuracy are not. Adequate approaches may include using single-component sensors, 1D crustal models, station corrections, compressional-waves only for locations, simple amplitude- or coda-length magnitudes, and the shear-faulting-only assumption to derive fault-plane solutions.

Such approaches are not, however, adequate to deliver the levels of accuracy, either in results or in error estimates, that modern industrial hydraulic fracturing applications demand. These may include, for example, hypocenter locations accurate to a few meters in cases where earthquake locations are used to guide drilling. For these purposes, specialist approaches are necessary. In this paper,

Manuscript received by the Editor 9 March 2011; revised manuscript received 16 May 2011; published online 6 January 2012.
[1]University of Durham, Department of Earth Sciences, Science Laboratories, South Road, Durham, U. K. E-mail: g.r.foulger@durham.ac.uk, b.r.julian@durham.ac.uk.

we provide a brief overview of some aspects of the advanced, state-of-the-art methodologies that can deliver results to the required standards. We focus particularly on surface seismometer arrays deployed to monitor hydraulic fracturing in geothermal settings.

EARTHQUAKE LOCATIONS

Maximizing location accuracy

Hypocentral locations are arguably the most fundamental information about earthquakes. Nevertheless, hypocenters are often surprisingly poorly determined. Even when earthquakes actually lie on planar structures, computed hypocenters typically show only diffuse "dots in a box," and have limited ability to reveal geological features such as faults that may be important drilling targets. Furthermore, derived hypocenters are often subject to significant systematic biases, causing clouds of locations to be displaced from their true positions. The problem for the end user may be exacerbated where independently computed locations differ by more than the stated formal errors. This inconsistency results from the errors being calculated incorrectly, ignoring what is often the major contributor to the error budget, which is uncertainty about crustal structure. As a result, there is an urgent requirement for tools that produce locations that are not only accurate, but also have realistic error estimates.

Seismic network design

A geometrically well-distributed network of 3C seismometers is a prerequisite for computing hypocenters accurately. Ideally, seismometers should surround the earthquakes uniformly in three dimensions, and include stations below the events, but this is not usually practical. In general, a distributed, near-surface array is the closest approximation to this that can economically be achieved.

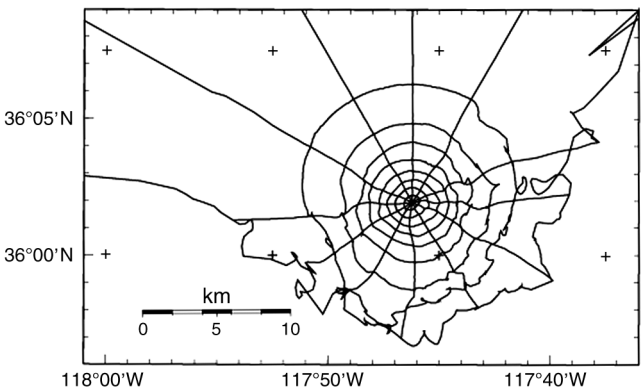

Figure 1. Map showing the surface projection of the upper focal hemisphere of an earthquake 3 km deep at the Coso geothermal field, computed using a 3D crustal model (Wu and Lees, 1999). The quasi-radial lines have constant take-off azimuths spaced 30° apart. The quasi-concentric curves have constant "incidence angles," measured from nadir, spaced 10° apart. The small-scale complexity of the pattern for rays departing toward the south and southeast reflects the sensitivity of raypaths to structural details in the model. Similarly, the simplicity of the pattern for rays to the northwest reflects a lack of structural information in that part of the model.

Deploying strings of sensors in multiple boreholes is also a good approach, but usually prohibitive on grounds of expense.

Where the earthquakes of interest are small or ground noise, e.g., from operations, is high, near-surface sensors may be unable to record events of interest sufficiently well to contribute data to locations. In some experiments, strings of sensors in boreholes are used. With such an approach, it may be possible to deploy instruments within a few hundred meters of the earthquakes of interest. However, a single linear string of sensors is a geometrically weak configuration, which limits potential hypocentral accuracies. The network geometry can be improved by deploying strings in several boreholes. This is expensive, and thus rarely done, and brings with it increased uncertainties in sensor positions and orientations if the boreholes are deep (Bulant et al., 2007).

The stations of near-surface arrays should preferably be installed in boreholes at least a few tens of meters deep that traverse superficial layers of unconsolidated material and penetrate bedrock. Experience in geothermal areas shows that such deployment tends to reduce noise from operations, weather, and seismic-wave reverberations in soft shallow layers.

Seismometers should be distributed uniformly over the upper focal hemisphere, the top half of a conceptual sphere surrounding an earthquake hypocenter, through which seismic waves pass on their way to stations. The accuracies of both hypocenter locations and moment tensors are enhanced if the focal sphere is well sampled by rays.

In real situations, crustal structure is not homogeneous. As a result, seismic wavefronts from earthquakes are distorted from ideal shapes. Seismic waves leaving the hypocenter and penetrating the upper focal hemisphere thus do not impinge on the surface of the earth in a regular, symmetric way. This must be taken into account in the placing of seismic stations if an optimal geometry is to be achieved. Figure 1 shows the upper focal hemisphere of an earthquake hypocenter mapped onto the earth's surface. The distortion of the impinging wavefronts was calculated by tracing rays through a 3D crustal model derived earlier using local-earthquake tomography. To achieve uniform coverage of the focal sphere, the stations of near-surface arrays should be sited with reference to calculations of seismic-ray distortion of this sort. This method has so far been applied to two geothermal areas (Miller et al., 1998; Julian et al., 2009).

Crustal models

In the case of well-designed networks, the dominant source of location error in geothermal areas is usually imperfectly known crustal structure (e.g., Maxwell, 2009). Whereas random errors associated with timing and arrival-time measurements may result in a few tens of meters of error in locations, the systematic errors that result from poor knowledge of crustal structure may be several times larger. There are several ways of reducing this problem.

Initial, 1D models are generally obtained using controlled-source seismology. To penetrate to several kilometers depth in refraction experiments, profiles several tens of kilometers long, and relatively large explosions are needed. Sophisticated experiments involving many profiles and multiple explosions are necessary to acquire spatially extensive, 3D crustal models from such work. In oil and gas reservoirs, sophisticated 3D seismic reflection surveys are sometimes done to obtain accurate crustal structure information, but this is rarely done in geothermal areas. In those environments,

usually, a few profiles only are shot and the result is a relatively simple, 1D model.

Such models may be improved using the local earthquakes themselves. One-dimensional inversions are conducted of arrival-times from shots (explosions for which the origin time is not measured), explosions (explosions for which the origin time is measured) and earthquakes, to calculate the 1D crustal model that minimizes the root-mean-square misfit of the arrival-time measurements (e.g., Kissling, 1995). Locating earthquakes using 1D models improved in this way may reduce location errors by a few percent.

If earthquakes are well-distributed beneath a seismometer network, it may be possible to use local-scale seismic tomography to determine a 3D crustal model. Seismic tomography has been successfully applied to several exploited volcanic and geothermal areas (Foulger and Toomey, 1989; Foulger and Arnott, 1993; Arnott and Foulger, 1994; Foulger et al., 1995a, 1995b; Julian et al., 1996; Ross et al., 1999).

In such areas, it is not uncommon for wave speeds to vary laterally on a scale of kilometers by more than 10%. The resulting traveltime anomalies may then be an order of magnitude larger than measurement errors and dominate the hypocentral-location error budget. Significant errors may also be introduced into moment-tensor solutions if this affect is not accounted for (Foulger and Julian, 1993). Tomographic inversions typically solve for corrected hypocenter locations, in addition to a 3D crustal model. Locating local earthquakes using such a model can greatly reduce these errors. In practice, only errors resulting from inhomogeneities on the scale of structural parameterization are reduced. This is typically 1–2 km at best.

A variety of physical processes can cause the large-scale structure in geothermal and hydrocarbon reservoirs to vary with time. These include changes in the stiffness of the rock matrix caused by drying or wetting of clay minerals (e.g., Boitnott and Boyd, 1996), changes in pore-fluid compressibility caused by CO_2 flooding (e.g., Wang et al., 1998; Daley et al., 2007) and fluid extraction (e.g., Gunasekera et al., 2003). Particularly strong changes in V_P/V_S occurred in The Geysers geothermal reservoir, California in the 1990s, as a result of production of steam and consequential drying of the geothermal reservoir. Changes in anisotropy are also commonly observed in hydrocarbon reservoirs (e.g., Al-Harrasi et al., 2011; Meersman et al., 2009).

Temporal changes in structure can be detected using conventional tomography methods to invert seismic-wave arrival-time data sets for different epochs independently. This approach is only reliable under ideal experimental conditions, however. This requires that the area is continuously seismically active and has been monitored by a dense, high-quality seismic network for a period spanning major operations. Most situations fall short of this ideal. In those cases, the assumption that differences in tomographic structure calculated independently from year to year correspond to real changes in structure is unsafe. The results of repeated tomography experiments differ even if the structure does not change, simply because of variation in the seismic ray distribution caused by natural variation in earthquake locations (Foulger et al., 1995a). These problems have been addressed by the recent development of a new tomography method, *tomo4d*, which inverts multiple data sets simultaneously, imposing constraints to minimize the differences between the models for different epochs (Julian and Foulger, 2010).

Calibration explosions

Only one method can almost completely eliminate errors due to poorly known crustal structure in the case of regions of interest on the scale of kilometers. This is to use calibration explosions to determine exact traveltime corrections corresponding to the raypaths between the earthquake source volume and each seismic station. In the simplest case, a single explosion is fired in a borehole, near to the anticipated position of the hydraulic-fracturing induced earthquakes. This explosion is recorded on the seismic stations of the network that will monitor the earthquakes. An alternative, equivalent approach that avoids the necessity of firing a shot in the borehole is to deploy a sensor downhole and to fire timed explosions at each seismic station. This technique is currently in the early pioneer stage at geothermal areas monitored by surface seismometer arrays.

Absolute traveltimes for waves traveling between the anticipated seismogenic volume and the stations may then be measured. These may be compared with the traveltimes calculated using the best crustal model available. The differences between the two sets of traveltimes represent corrections that must be applied to earthquake arrival times, to correct for the imperfection of the crustal model.

Relative locations

Relative hypocenter location methods can greatly reduce the errors in location between individual earthquakes in a cluster, thereby improving the resolution of seismically active structures (e.g., De Meersman et al., 2009; Jansky et al., 2009). It is important to realize, that the *absolute* location of the entire cluster is not improved by this method, but only the errors in the differences between earthquake locations.

Relative location methods use, for each seismic station, the differences in arrival times of waves from closely spaced earthquakes. For such earthquakes, the biases caused by imperfectly modeled geological structure along the raypaths are almost identical. They thus nearly cancel out when arrival times are differenced, and the variations in arrival times remaining are largely a result of true, small variations in location between the earthquakes (Waldhauser and Ellsworth, 2000). The relative location method can be applied to arrival times obtained using any method, including automatic measurements, hand-measurements, and arrival times improved by waveform crosscorrelation. Waveform crosscorrelation is most helpful where waveforms are similar, and may be included automatically in the relative-location process. The results of relatively relocating events in a tight cluster can be a spectacular improvement in the clarity of delineated structures — a move from "dots in a box" to "faults in a box" (Julian et al., 2010b) (Figure 2).

Assessment of hypocentral uncertainty

Just as important as accurate hypocenter locations are reliable assessments of their accuracy, an aspect of earthquake seismology that is still an area of active research. By far the most common method of estimating hypocenter locations involves fitting the arrival times of seismic body-wave phases such as P and S using conventional least-squares methods (e.g., Aki and Richards, 1980, Box 12.3; Press et al., 2007, Chapter 15). Implicit in the use of least-squares fitting is the assumption that the errors in the data are normally distributed. For a linear (or, as in this case, linearized) inverse problem, the derived parameters are then (asymptotically, as the

confidence level decreases to zero) normally distributed and their joint confidence regions are (asymptotically) hyperellipsoids. Furthermore, if the data errors are statistically independent and equal (or if their relative magnitudes are known), then their values can be estimated from the quality of the least-squares fit obtained.

It has long been evident, however, that the hypocentral confidence regions computed by most commonly used earthquake-location programs are unrealistic. In an early, but very careful, computer-based study of the subject Flinn (1965) obtained a mean depth of 39 ± 2 km for 12 nuclear explosions that had been fired just below the surface in Nevada. Numerous subsequent studies using increasingly large high-quality data sets and increasingly sophisticated analysis methods gave similar results (for example, Chang et al., 1983; Yang et al., 2004).

The cause of such absurdly optimistic confidence estimates lies in two frequently made but incorrect assumptions: that hypocentral errors are caused entirely by observational (seismogram-reading) errors, and that the errors for different observations are statistically independent. These assumptions confer significant computational advantages. The $m \times m$ covariance matrix $\mathbf{S}$ of the observational errors (see below) becomes diagonal, with only m independent elements, where m is the number of observations, and inverting $\mathbf{S}$ becomes trivial. Because of the greatly enhanced computing power now commonly available, these computational advantages are, however, no longer as important as they once were.

In reality, for experiments on the scale of kilometers, variations in traveltimes caused by the imperfectly known structure of the earth usually are much larger than observational errors. More importantly, these structure-related errors are strongly correlated: raypaths from an event to seismometers near one another are close together, and their associated traveltimes are affected similarly by heterogeneities in the seismic wave speeds. In such cases, hypocenter-location algorithms can commonly reduce the arrival-time residuals by "mislocating" the earthquake. For example, if wave speeds are generally higher to the east than to the west of an earthquake, the arriving waves will be earlier to the east than at the same distances to the west, and they will "pull" the computed location to the east. Such mislocation produces a fit to arrival-time data that is deceptively good, and leads to unrealistically small computed confidence regions.

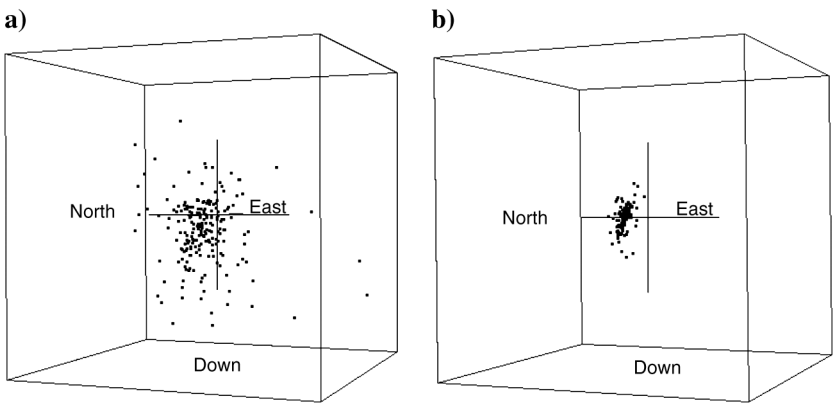

Figure 2. Left: Conventionally determined individual earthquake locations (dots in a box); right: relative relocations (faults in a box). But do we know the absolute location of the new fault well enough to drill through it? The green box is $4 \times 4 \times 4$ km in size, and the white cross is $2 \times 2 \times 2$ km from side to side.

An occasionally used and simple, but approximate, solution to this problem is to use a priori standard errors for data when estimating hypocenters, and to make these values large enough to account for both the reading errors and traveltime uncertainties (Julian, 1973). The covariance matrix is still diagonal, so negligible extra computational effort is required. This tactic is not ideal, however. It enlarges the sizes of the computed confidence regions, but does not change their shapes, as it should to account for the effect of traveltime correlation. We outline an improved strategy below.

In addition to distorting the sizes and shapes of computed confidence regions, the spatial correlation of traveltime anomalies also biases computed hypocenters. This effect results from the inevitably nonuniform distribution of observable seismic rays around hypocenters. The rays oversample the wave-speed anomalies in some directions and these rays therefore have a disproportionate effect and introduce bias into computed hypocenters.

To avoid this difficulty, we propose incorporating into hypocenter-location methods a stochastic model of traveltime anomalies caused by earth heterogeneity. This tactic can greatly improve the quality both of hypocentral estimates, and of computed hypocentral confidence regions.

Method

Arrange the four origin coordinates (three spatial coordinates and origin time) of an earthquake in a column vector $\mathbf{x}$, and similarly arrange the m observed arrival-time residuals (observed minus predicted times) with respect to an assumed origin in a column vector $\mathbf{b}$. The functional relation between the origin coordinates and the predicted arrival times is nonlinear, and the standard solution method is to iteratively solve a linearized problem in which small changes in the origin $\delta\mathbf{x}$ are related to predicted changes $\delta\mathbf{b}$ in the residuals by a linear operator (the first term of a Taylor-series expansion). A good starting guess is necessary. This operator takes the form of an $m \times 4$ matrix $\mathbf{A}$, such that first-order changes in the residual vector are given by the "design equations"

$$\delta\mathbf{b} = -\mathbf{A}\delta\mathbf{x}. \quad (1)$$

In least-squares fitting, we seek to minimize the quantity

$$\chi^2 = (\mathbf{A}\delta\mathbf{x} - \mathbf{b})^T\mathbf{S}^{-1}(\mathbf{A}\delta\mathbf{x} - \mathbf{b}), \quad (2)$$

where the superscript T indicates vector/matrix transposition and $\mathbf{S} = \langle\mathbf{b}\mathbf{b}^T\rangle$ is the symmetric $m \times m$ covariance matrix of the observational errors. The bracket symbols $\langle\rangle$ indicate the mathematical expectation of a random variable.

Most existing hypocenter-location programs assume that the errors in the observed arrival times are statistically independent, so that the covariance matrix $\mathbf{S}$ is diagonal, with elements equal to the variances of the m observations:

$$S_{ij} = \sigma_i^2\delta_{ij} \text{ (no summation over } i). \quad (3)$$

In this case, the effect of the covariance matrix $\mathbf{S}$ in equation 2 is to divide each design equation by the corresponding standard error, σ_i, which is equivalent to weighting each design equation by

the quantity $1/\sigma_i^2$. Frequently, programs constrain the relative values of the standard errors σ_i, and use the best-fit value of χ^2 to estimate their overall level, a procedure that would be justified if the errors were statistically independent. However, this leads to hypocentral bias and misleading confidence estimates when they are not, for reasons explained above. A possible solution to this problem is to recognize that the error in each observed arrival time δt has two components: a true measurement error δt^m, and a traveltime anomaly δt^a

$$\delta t = \delta t^m + \delta t^a. \tag{4}$$

This approach leads to a nondiagonal covariance matrix in the least-squares fitting problem, and inverting such a matrix requires $O(m^3)$ operations, which even today may be prohibitive for problems with many hundreds of observations. Many current industrial applications, however, involve tens of observations, so inverting the full covariance matrix in these cases is practical.

Rodi and Meyers (2008) recently undertook such an approach, estimating the statistics of δt^a for long paths (up to 3000 km) from models of earth's crust and upper mantle. We propose here an approach that may be more appropriate for the short paths relevant to industrial applications, treating the wave speeds as spatially constant with additive stochastic perturbations.

A stochastic model of traveltime anomalies

The traveltime along a ray is

$$t = \int_0^L s(\mathbf{r}(l))\mathrm{d}l, \tag{5}$$

where $s(\xi)$ is the wave slowness (inverse of wave speed) as a function of position ξ and $\mathbf{r}(l)$ is the parametric representation of the raypath, with the parameter l being path length and ranging from zero to L along the ray.

Now let the slowness field $s(\xi)$ consist of two components: a deterministic component $s_0(\xi)$, upon which the earthquake location computations are based, and a random perturbation $\delta s(\xi)$, about which only statistical information is available: $s(\xi) = s_0(\xi) + \delta s(\xi)$. The perturbation δs will cause a first-order change in the raypath, but to a first-order the change in the traveltime can be computed using the unperturbed raypath

$$\delta t^a \approx \int_0^L \delta s(\mathbf{r}(l))\mathrm{d}l \tag{6}$$

(Julian and Anderson, 1968). The covariance of these traveltime perturbations along two different raypaths $\mathbf{r}^{(1)}$ and $\mathbf{r}^{(2)}$, of lengths P and Q, can be expressed as

$$\begin{aligned}\langle \delta t^{a(1)} \delta t^{a(2)} \rangle &\approx \left\langle \int_0^P \delta s(\mathbf{r}^{(1)}(p))\mathrm{d}p \int_0^Q \delta s(\mathbf{r}^{(2)}(q))\mathrm{d}q \right\rangle \\ &= \int_0^P \int_0^Q \langle \delta s(\mathbf{r}^{(1)}(p)) \delta s(\mathbf{r}^{(2)}(q)) \rangle \mathrm{d}p\mathrm{d}q. \end{aligned} \tag{7}$$

Introducing the *correlation function* of the slowness perturbations $R(\mathbf{a}, \mathbf{b}) = \langle \delta s(\mathbf{a}) \delta s(\mathbf{b}) \rangle$, we get

$$\langle \delta t^{a(1)} \delta t^{a(2)} \rangle \approx \int_0^P \int_0^Q R(\mathbf{r}^{(1)}(p), (\mathbf{r}^{(2)}(q))\mathrm{d}p\mathrm{d}q. \tag{8}$$

The correlation function $R(\mathbf{a}, \mathbf{b})$ contains all the statistical information needed to compute the contribution of traveltime uncertainties to the covariance matrix $\mathbf{S}$. Computing this double integral using complete raypaths for every pair of observations would be laborious, even if all the required information, such as the function $R(\mathbf{a}, \mathbf{b})$, were available. To simplify the problem, we approximate the raypaths as straight-line segments and also assume that the correlation function depends only upon the vector difference of its arguments (is spatially stationary), and further, that it depends only on the length of the difference vector (which is spatially isotropic)

$$R(\mathbf{a}, \mathbf{b}) = R(r), \quad \text{where } r = |\mathbf{a} - \mathbf{b}|. \tag{9}$$

We assume a mathematically tractable exponential analytic form for R,

$$R(r) = \sigma^2 e^{-r/a}, \tag{10}$$

where σ is the standard deviation of the slowness and a is its "correlation distance," which may be thought of as the typical size of the slowness heterogeneities. Actually, this assumption involves a significant oversimplification. In reality, the correlation distance usually is greater in horizontal directions than in the vertical direction, especially in sedimentary basins. We only intend to outline a general approach here, not a fully developed theory.

Even with these simplifying assumptions, it is not possible to express the covariance of the traveltimes in closed form as a function of the angle α between the rays and their length L, which we take as the same for both rays in a pair. We can, however, determine the approximate shape of this function. If the angle $\alpha = 0$, then the rays are coincident and the variance of the traveltime is

$$\langle (\delta t)^2 \rangle = 2\sigma^2 a^2 \{ e^{-L/a} + L/a - 1 \}. \tag{11}$$

For short paths ($L/a \ll 1$) this function is quadratic, with $\langle (\delta t)^2 \rangle \approx \sigma^2 L^2$, and for long paths ($L/a \gg 1$) it is linear, with $\langle (\delta t)^2 \rangle \approx 2\sigma^2 a L$. For rays departing in opposite directions ($\alpha = \pi$) the covariance $\langle \delta t_1 \delta t_2 \rangle = \sigma^2 a^2 (1 - e^{-L/a})^2$. Figure 3 shows the covariance function for these cases. For infinitely long paths, the covariance is

$$\begin{aligned}\langle \delta t_1 \delta t_2 \rangle &= \sigma^2 a^2 \int_0^\infty \left[\int_0^\infty e^{-\sqrt{x^2 + y^2 - 2xy \cos \alpha}} \mathrm{d}x \right] \mathrm{d}y \\ &= \sigma^2 a^2 \frac{\pi - \alpha}{\sin \alpha} \end{aligned} \tag{12}$$

(Figure 4). This function increases without limit as $\alpha \to 0$, but for finite path lengths it must be bounded by the values given by equation 12, indicated by dotted lines on Figure 4. The use of a full covariance matrix, even one based on an ad hoc combination of the curves and dotted lines of Figure 4, will yield major improvements in both hypocentral accuracy and in the accuracy of computed hypocentral confidence regions. Improving our knowledge about the actual statistics of structural fluctuations in the earth will yield even greater improvements.

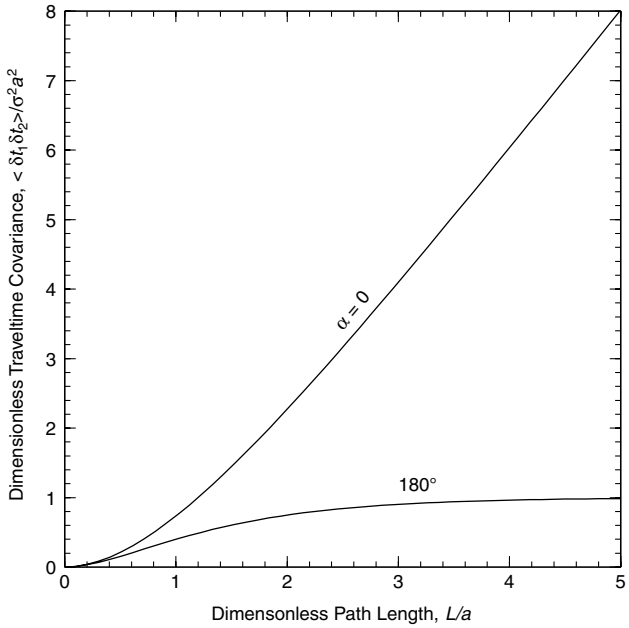

Figure 3. Covariance of traveltime along straight-line paths as a function of path length, for two values of the angle α between the paths, for a stochastic medium having an exponential correlation function of wave-slowness heterogeneities. Path length is normalized by a, the correlation distance of the heterogeneities. Traveltime variance is normalized by a^2 and by σ^2, the variance of the wave-slowness heterogeneities.

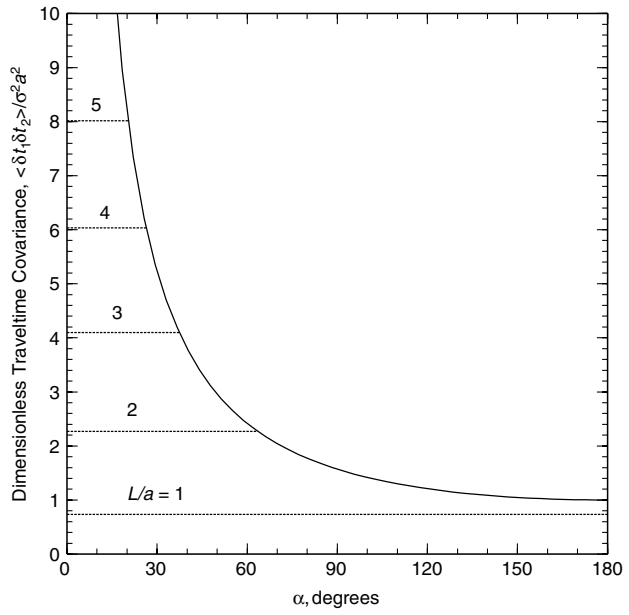

Figure 4. Covariance of the traveltimes along two different paths, as a function of the angle α between the paths, for an exponential correlation function of the wave-slowness heterogeneities. The paths are taken to have infinite lengths, so the covariance increases without limit as $\alpha \to 0$. For finite-length paths the covariance is bounded, as shown by the upper curve in Figure 3. The horizontal dashed lines on the left show the bounding values for different values of dimensionless path length, L/a. Traveltime covariance is normalized by a^2, the square of the correlation distance of the heterogeneities, and by σ^2, the variance of the wave slowness.

EARTHQUAKE MAGNITUDES

The sizes of earthquakes were originally expressed using magnitude scales defined in terms of seismogram characteristics, not source characteristics. This is the basis for scales such as the local (or "Richter") magnitude scale, for example. They are poorly suited for industrial work for a number of reasons. They result in the magnitude of an earthquake varying from seismogram to seismogram, and the seismic phase measured is sometimes not defined, so it is impossible, even in principle, to improve measurements of M_L as knowledge improves about the earth and about seismic-wave propagation. Empirical magnitude scales for local networks are often constructed by correlating measured wave amplitudes with magnitudes from existing regional stations. This requires downward extrapolation over several magnitude units to apply them to microearthquakes, potentially resulting in large systematic variations between different scales.

The most accurate measure of earthquake size, and the one that should be used, is the low-frequency scalar seismic moment, M_0. Seismic moment is a measure of earthquake size that is based on fundamental physics of the source, and not simply seismogram characteristics. Because M_0 varies by more than a factor of 10^{18}, it is conventional to define a logarithmic moment-magnitude

$$M_W = \frac{2}{3} \log M_0 - 10.7, \tag{13}$$

where M_0 is measured in Newton-meters (Kanamori, 1977; Hanks and Kanamori, 1979). For simple shear faulting, $M_0 = \mu A \bar{u}$, where μ is the rigidity modulus at the hypocenter, A is the fault area, and $\bar{u}$ is the average displacement on the fault. For more general source types, seismic moment is regarded as a symmetric tensor with elements M_{ij}. The scalar moment is $M = \sqrt{\frac{1}{2}\sum_{i,j=1}^{3} M_{ij}^2}$ (Silver and Jordan, 1982), and M_0 is the low-frequency limit of M. The theory of the excitation of elastic waves by moment-tensor sources is well developed (e.g., Aki and Richards, 2002, equations 4.29, 4.97, 7.148–7.150), so determining moment magnitude depends only on our knowledge of the propagation medium and our ability to solve the wave equation. Moment magnitude thus anticipates, rather than precludes, exploitation of advances in knowledge.

SOURCE MECHANISMS

Seismic failure can involve several physical processes that are important in hydrocarbon or geothermal reservoirs. These include (1) simple shear slip on planar faults, (2) tensile cracking, (3) simultaneous shear slip and/or tensile cracking on multiple faults, and (4) rapid fluid motion. To these might be added artificial sources such as (5) explosions, which can additionally trigger all of the above processes. Traditional seismological "fault-plane solutions," based on the "double-couple" equivalent force system, describe only the first of these processes, and then only under simplifying assumptions about rock homogeneity and isotropy. The more general moment-tensor source model of seismic source mechanisms can represent any combination of processes (1), (2), and (3), and offers in addition the computational advantage of a linear theory for seismic-wave excitation.

Fault-plane solutions usually are derived from the polarities of first-arriving compressional waves (P phases). If these polarities are projected back along seismic rays to an infinitesimal "focal

sphere" surrounding the hypocenter, the simple-shear-faulting (double couple) model predicts that compressional and dilatational polarities (outward and inward motions) will occupy alternating quadrants separated by a pair of orthogonal great circles. One of these defines the fault-plane. The only property a fault-plane solution has, therefore, is its orientation. Furthermore, the fault-plane solution does not identify which great circle represents the fault and which the "auxiliary plane."

Obtaining accurate fault-plane solutions from *P*-phase polarities requires dense sampling of the focal sphere. In the case of surface arrays, examination of real data suggest that networks of 20 to 30 well-distributed seismometers are sufficient (Miller et al., 1998). When, as is commonly the case in routine seismic monitoring of geothermal areas, fewer stations are used (sometimes fewer than 10), errors in the orientation of the derived fault plane, and in the direction of slip, may be several tens of degrees.

In the 1980s, some earthquakes in volcanic and geothermal areas were found to have non-double-couple source mechanisms (Julian, 1983; Foulger and Long, 1984; Foulger et al., 1989). These required volume changes caused by the opening or closing of cracks or other cavities, and more general kinds of shear deformation, which might indicate tensile cracking or simultaneous shear slip on multiple faults. The first such discoveries involved events with large non-double-couple components and dense seismometer networks. As high-quality seismometer networks in such environments became more numerous, however, reports of non-double-couple source mechanisms became more common and various methods were developed for inverting observed data to retrieve them (e.g., Šílený et al., 1992). Seismic studies of mines also detected non-double-couple earthquake mechanisms (e.g., Feignier and Young, 1992; McGarr, 1992). Studying such sources can yield information of potential operational value, distinguishing, for example, shear-faulting from crack opening and closure. For earthquakes induced by EGS-related hydraulic fracturing, moment-tensor mechanisms can reveal the nature of the fractures created or reactivated.

Non-double-couple source mechanisms are difficult to identify using *P*-phase polarities alone, however. Even with dense seismometer networks, such data usually are highly ambiguous (Julian et al., 1998). Additional information is needed, which can include either full waveforms (e.g., Dreger and Helmberger, 1993) or, more simply, the polarities and amplitudes of *P*- and *S*-phases (Julian and Foulger, 1996). The polarities of horizontally polarized shear waves (S_H) are fairly easy to determine because S_H and P/S_V waves are only weakly coupled (under idealized conditions they are uncoupled), but for instruments distributed on the surface S_H polarities provide much more information than *P* polarities do.

The shapes alone of even a small number of seismic waveforms may contain enough information to resolve the complete moment tensor of a seismic event. Existing waveform-inversion methods (Dreger and Helmberger, 1993), however, are applicable only to comparatively large earthquakes recordable at regional distances. For small earthquakes such as those induced by hydraulic fracturing, a practical method is inversion of P- and S-wave polarities and amplitude ratios (Julian and Foulger, 1996). Like waveforms, amplitude ratios can be less severely distorted by wave-propagation anomalies than are amplitudes themselves because effects such as anelastic attenuation and geometric spreading behave similarly for appropriately chosen paths, reducing their distorting effect upon the corresponding ratios. Using this method, good results may be obtained with networks containing 10–15 3C seismometers. The separate channels must have well matched (or at least well known) gains and known orientations. If borehole sensors are used, they must meet these requirements.

Displaying moment tensors graphically, including both source types and orientations, requires complicated plots that are difficult to understand. Therefore, separate plots are usually used, one displaying source-type information only (Hudson et al., 1989) (Figure 5 — top), and the other displaying only orientation information (Figure 5 — bottom).

Moment tensor analysis has now been used to study the source mechanisms of many natural and industrially induced earthquakes. These include several geothermal and hydrocarbon reservoirs areas and EGS stimulation experiments (Julian and Foulger, 1996; Ross et al., 1996; Julian et al., 1997; Miller et al., 1998; Šílený et al., 2009; Baig and Urbancic, 2010; Julian et al., 2010b).

Interpreting moment tensors and hypocenter locations jointly

Interpreting moment tensors in terms of physical processes is, unfortunately, nonunique. Different source processes can produce identical seismic wave fields, and thus have identical moment tensors (Julian et al., 1998). For example, the deviatoric part of any moment tensor can be decomposed into a pair of double-couple (shear-faulting) sources, or alternatively, into a combination of a (different) double couple and a CLVD. Even worse, neither type of decomposition is unique. More information than the moment tensor provides is thus needed to reduce this ambiguity.

One useful approach is to interpret moment tensors along with structural information obtained from earthquake locations. Relatively located hypocenters can provide high-resolution images of the spatial distributions of earthquakes, revealing the geometry of seismic failure regions.

We have applied this method to two cases so far. In 1997, a swarm of earthquakes in the south moat of Long Valley caldera, west of Casa Diablo Hot Springs was recorded by a network of 69 digital, 3C seismic stations (Foulger et al., 2004). Well-constrained moment tensors obtained for several of these earthquakes have mechanisms that are close to double couples, but contain a net volume increase. High-resolution relative hypocenter locations for the entire sequence of several hundred earthquakes clearly define a failure plane that bisects the dilatational polarity fields of the earthquake radiation patterns. This fact rules out shear faulting and requires that the primary failure mechanism is tensile cracking, probably caused by hydraulic fracturing (Foulger et al., 2004).

In the second case, a hydraulic injection in the Coso geothermal area in 2005 induced a swarm of several tens of microearthquakes. Relative locations determined using 27 surface and shallow-borehole 3C seismometers delineate a clear fault plane, 600 m in length, striking N 20 °E, and dipping at 75° to the west-northwest. Surface geology and borehole televiewer observations show that this plane coincides with a preexisting fault. The earthquakes had similar non-double-couple mechanisms involving volume increases, and the fault plane bisects the dilatational *P*-phase polarity fields (Julian et al., 2010a) (Figure 6). The additional constraining information from the orientation of the fault plane shows that the source process was dominated by tensile failure.

Confidence bounds for moment tensors

Source mechanisms such as those shown in Figure 5 and Figure 6 are of little use without additional information about their probable uncertainties. Inevitable errors in measuring wave polarities and amplitudes are mapped in a complicated manner into errors in the derived moment tensors. If these errors are strongly correlated, they might produce systematic artifacts that could be mistaken for real geophysical phenomena. To date, only a few moment-tensor analyses have included any kind of error analysis (Baker and Young, 1997; Trifu et al., 2000; Šílený et al., 2009; Baig and Urbancic, 2010).

We therefore extended the linear-programming method of Julian and Foulger (1994) to compute confidence regions for moment tensors. After finding the minimum value of an objective function that measures the L1 norm of the residuals between the observed and computed polarities and amplitude ratios, we constrain this objective function to lie below a somewhat larger value chosen on the basis of a priori estimates of uncertainty caused by measurement errors and earth-model uncertainty. We then move the solution in 6D moment-tensor space in various specified directions as far as the constraint allows. In this way, we obtain a suite of solutions that fit the data adequately (Figure 7).

Results from applying this method to amplitude-ratio data from several geothermal areas in Iceland, Indonesia, and California show that moment-tensor confidence regions often, but not always, are elongated along a trend between the +Dipole and −Dipole points on the source-type plot. This observation suggests that part of the systematic trend that is frequently found for geothermal earthquakes may be an artifact of measurement error. For earthquakes that comprise a combination of shear slip and tensile crack opening, a distribution along a trend between the +Crack and −Crack points is predicted theoretically (Julian et al., 1998). Further work is required to fully understand why the moment tensors of natural earthquakes do not follow this distribution also. Importantly, error assessments need to be incorporated into routine moment-tensor results, both to give more information on the reliability of the results, and to build a set of case histories that may be used to increase our understanding of the response of reservoirs to hydraulic fracturing.

This same analysis shows that volume changes are well resolved by polarity/amplitude-ratio data. The observation that the source mechanisms involve systematically smaller volume changes than are expected for combined shear-plus-tensile faulting, is thus apparently real — the trend between the +Dipole and −Dipole points on the source-type plot remains, even after error analysis. A volume-compensating process, such as rapid fluid flow into opening cracks, must thus be at work. Such unsteady fluid flow would contribute net forces to source mechanisms, which might be detectable by inversion methods that include lower-order

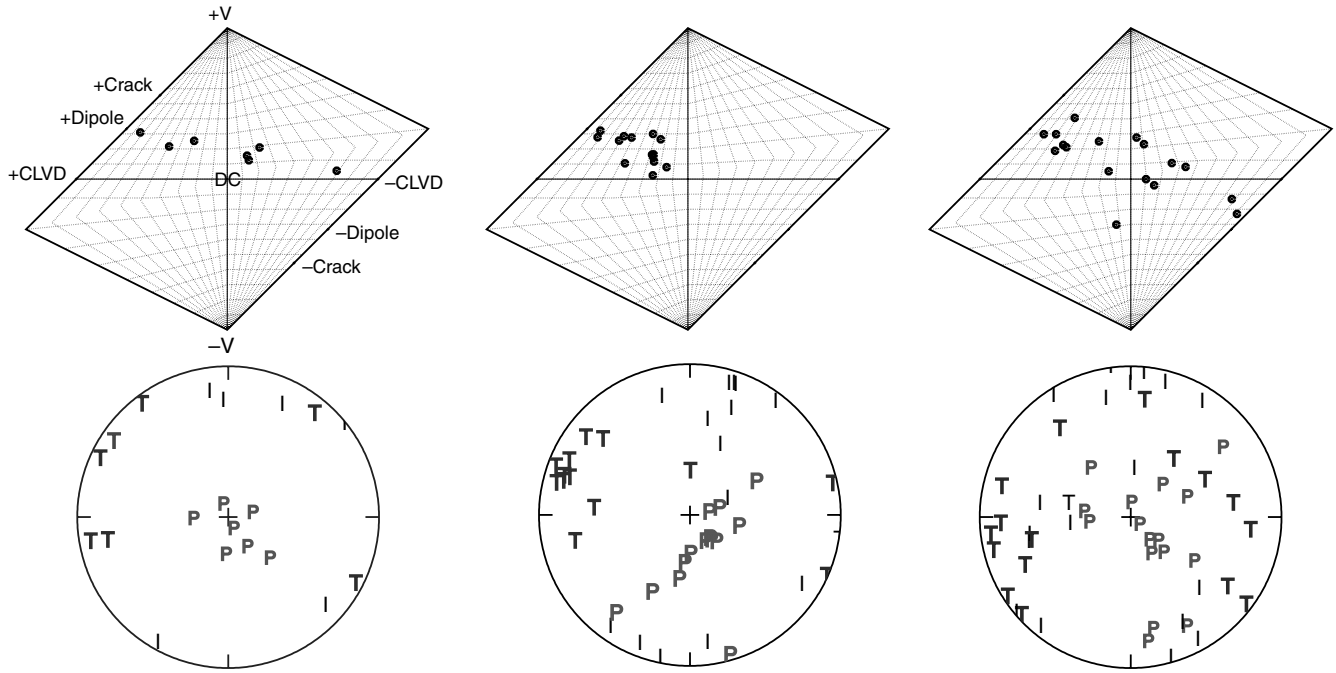

Figure 5. Moment tensor results for 37 earthquakes that were induced by a hydraulic injection in a borehole in the Coso geothermal field in 2005. Top: "Source-type" plots depict the moment tensor in a form that is independent of source orientation. All simple shear-faulting mechanisms, whether strike-slip, normal, or reverse, plot at the central point labeled DC (double couple). The vertical coordinate k measures volume change, and ranges from −1 at the bottom of the plot to +1 at the top. Mechanisms with volume increases lie above the horizontal line through the central point DC, and mechanisms with volume decreases lie below it. Pure (spherically symmetric) explosions lie at point +V and pure implosions lie at −V. The left-right coordinate T characterizes the type of shear deformation, and ranges from −1 on the left to +1 on the right side of the plot. Simple shears ($T = 0$) lie on the vertical line through the central point DC, and more complex pure shears lie to the right or left of this line. In particular, opening (closing) tensile cracks, which involve both shear and volumetric deformation, lie at the point +Crack (−Crack). The points ±CLVD and ±Dipole represent mathematically idealized force systems that could be caused by the opening or closing of cracks accompanied by volume-compensating fluid flow. Bottom: Pressure (P) and tension (T) axes for the pre-, co-, and postswarm earthquakes, plotted on upper-hemisphere stereographic projections. The P and T axes give a rough indication of the orientation of the greatest and least principal stresses, respectively.

moments (Backus and Mulcahy, 1976a, 1976b; Julian et al., 1998). Net forces may be significant components of earthquake mechanisms in geothermal and hydrocarbon reservoirs, and including them in source studies may contribute to understanding the volumetric components of geothermal and other reservoir-related earthquakes (Foulger et al., 2004).

The magnitudes of earthquakes are important in most industrial applications. Conventional magnitudes do not meet industrial standards. Moment magnitude should be used because it is related to fundamental physical processes at earthquake sources — it is not defined in terms of seismograms properties that ignore factors such as source and path effects.

DISCUSSION

Earthquake seismology has been used for a century to monitor regional earthquakes for academic and public hazard-reduction purposes. However, high accuracies and rigorous error estimates in hypocenter locations, magnitudes, and source mechanisms have tended to be neglected because they do not seriously influence decision-making for these applications. This is not the case for small-scale industrial applications, that include the mining industry and hydraulic stimulations, that have become a growing sector of earthquake seismology over the last several decades. In those cases, both high accuracies and correct error estimates are required. To achieve such accuracies, specialized experiment design is necessary — approaches traditionally used for regional monitoring do not suffice.

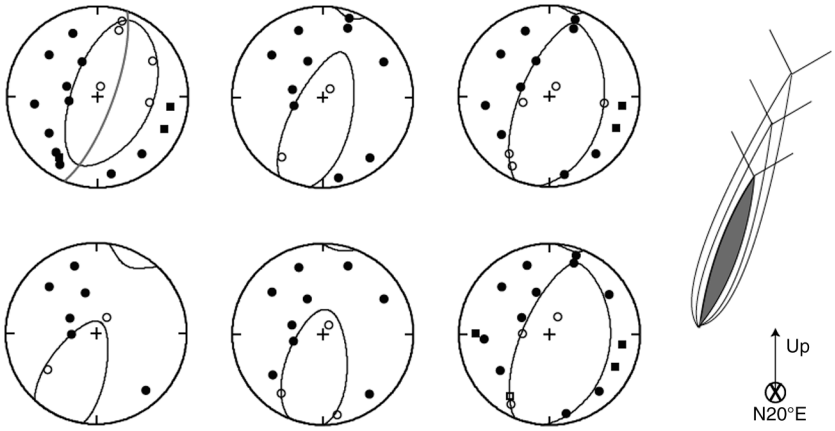

Figure 6. Moment tensors for six earthquakes from the 2005 hydraulic injection at the Coso geothermal area (from Julian et al., 2010a), displayed as P-wave polarity plots. Black lines: nodal curves. Red line: the fault plane delineated by relative hypocenter locations. Open/solid circles: dilatational/compressional arrivals; open/solid squares: dilatational/compressional arrivals, plotted at their antipodes; +: the center of the focal hemisphere. Upper focal hemispheres are shown in equal-area projection. Right: a schematic illustration of a suggested interpretation, a propagating tensile crack (gray) with shear wing faults.

Many modern geothermal industrial applications require hypocenter-location accuracies of meters or tens of meters. To achieve such accuracies, several design features must be incorporated into experiments, in particular in the case of near-surface seismometer arrays. Network geometry must take into account the crustal model, since this governs the mapping of seismic station locations onto the focal sphere. Sensors should preferably be deployed in boreholes, below poorly consolidated surface layers, to improve the signal-to-noise ratio. A crustal model as accurate as possible should be obtained, preferably a 3D model. Nevertheless, despite these measures, to reduce location errors to the level of a few meters or tens of meters, calibration explosions are required to obtain traveltime corrections corresponding to the specific source-station raypaths applicable to the planned experiment. Relative location methods can improve the accuracy of earthquake locations with respect to one another, thus improving the clarity of seismically active structures, but they do not improve the absolute location of the structure as a whole.

Rigorous uncertainty estimates are also needed. In the case of regional earthquake monitoring, little attention has traditionally been paid to the qualities of hypocenter locations because significant decisions have not depended on high accuracies. The most commonly used earthquake location programs assume that uncertainties are caused entirely by errors in the P- and S-wave arrival-time measurements, that these errors are statistically independent, and that simple arrival-time residuals give meaningful estimates of them. In fact, unknowns in crustal structure dominate the error budget, and must be accounted for in calculating hypocentral confidence regions. A hypocenter-location method based on a simple stochastic model of crustal heterogeneity, described in this paper, is applicable to industrial scenarios involving small seismometer networks and short raypaths.

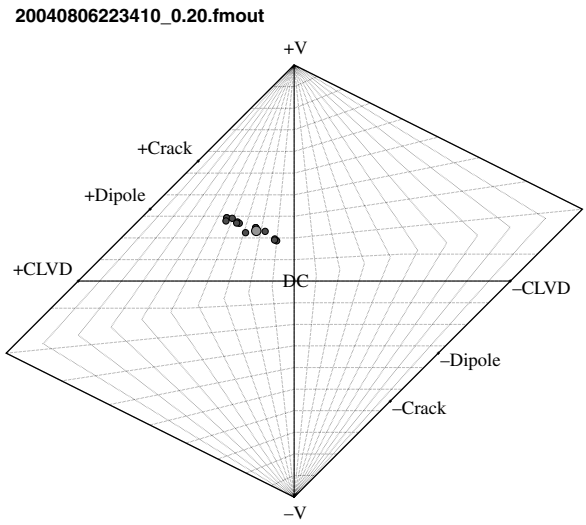

Figure 7. An example of confidence regions for the source type of a microearthquake at the Coso geothermal area, California. Light gray symbol: best-fit solution; dark gray symbols: other acceptable solutions that fit the observations within specified bounds. The resemblance of the confidence region to distributions sometimes observed for natural microearthquakes raises the possibility that such distributions may partially be measurement artifacts. The numerical bounds used here are arbitrary; choosing realistic bounds requires analysis of probable uncertainties in local structure, particularly with respect to anelastic attenuation.

In the case of source mechanisms, fault-plane solutions have been traditionally used for regional earthquake monitoring. This approach assumes shear slip on a planar fault surface and does not allow nonshear source components such as the opening and closing cracks, to be determined. To derive possible nonshear components, source mechanism studies must invert high-quality data for full moment tensors. The seismic networks that are suitable for such analyses are the same as those best suited for accurate locations. They comprise dense arrays of calibrated, 3C sensors, well-distributed over the focal sphere. Moment tensors are more complex to display graphically than simple fault-plane solutions. An effective approach is to use both a source-type plot, which displays the orientation-free information, along with a plot of *P*- and *T*-axes, which displays stress orientation information.

Interpreting moment tensors in terms of physical processes is fundamentally ambiguous. This ambiguity can be reduced by additional types of information. A promising approach is to infer structural information from relative hypocenter locations within earthquake sequences. These can provide independent constraints on the sizes, shapes, and orientations of causative structures. These, in turn, can be used to reduce the ambiguity in the sense of motion deduced from the moment tensors.

Realistic assessment of probable errors in derived moment-tensor source mechanisms is important to distinguishing spurious systematic trends from real physical source phenomena. A method involving calculating extremal solutions that fit the data within a priori estimates of measurement error is an effective way forward.

ACKNOWLEDGMENTS

This work was supported by many funding agencies over the years. We thank in particular recent support, which includes Department of Energy Awards No. DE-FG36-06GO16058 and DE-FG36-08GO18187 and support from the U.S. Navy Geothermal Program Office and the U.S. Geological Survey.

REFERENCES

Aki, K., and P. G. Richards, 1980, Quantitative Seismology. Theory and Methods: W. H. Freeman and Company.

Aki, K., and P. G. Richards, 2002, Quantitative Seismology (second edition): University Science Books.

Al-Harrasi, O. H., A. Al-Anboori, A. Wustefeld, and J.-M. Kendall, 2011, Seismic anisotropy in a hydrocarbon field estimated from microseismic data: Geophysical Prospecting, **59**, 227–243, doi: 10.1111/gpr.2011.59.issue-2.

Arnott, S. K., and G. R. Foulger, 1994, The Krafla spreading segment, Iceland: 1. Three-dimensional crustal structure and the spatial and temporal distribution of local earthquakes: Journal of Geophysical Research, **99**, 23801–23825, doi: 10.1029/94JB01465.

Backus, G., and M. Mulcahy, 1976a, Moment tensors and other phenomenological descriptions of seismic sources — II. Discontinuous displacements: Geophysical Journal of the Royal Astronomical Society, **47**, 301–329.

Backus, G., and M. Mulcahy, 1976b, Moment tensors and other phenomenological descriptions of seismic sources — I. Continuous displacements: Geophysical Journal of the Royal Astronomical Society, **46**, 341–361.

Baig, A., and T. Urbancic, 2010, Microseismic moment tensors: A path to understanding frac growth: The Leading Edge, **29**, 320–324, 10.1190/1.3353729.

Baker, C., and R. P. Young, 1997, Evidence for extensile crack initiation in point source time-dependent moment tensor solutions: Bulletin of the Seismological Society of America, **87**, 1442–1453.

Boitnott, G. N., and P. J. Boyd, 1996, Permeability, electrical impedance, and acoustic velocities on reservoir rocks from The Geysers geothermal field, Twenty-first workshop on geothermal reservoir engineering: Stanford University, **2**, 2–24 January 1996.

Bulant, P., L. Eisner, I. Psencik, and J. Le Calvez, 2007, Importance of borehole deviation surveys for monitoring of hydraulic fracturing treatments: Geophysical Prospecting, **55**, 891–899, doi: 10.1111/gpr.2007.55.issue-6.

Chang, A. C., R. H. Shumway, R. R. Blandford, and B. W. Barker, 1983, Two methods to improve location estimates — Preliminary results: Bulletin of the Seismological Society of America, **73**, 281–295.

Daley, T. M., R. D. Solbau, J. B. Ajo-Franklin, and S. M. Benson, 2007, Continuous active-source seismic monitoring of CO_2 injection in a brine aquifer: Geophysics, **72**, no. 5, A57–A61, doi: 10.1190/1.2754716.

De Meersman, K., J.-M. Kendall, and M. van der Baan, 2009, The 1998 Valhall microseismic data set: An integrated study of relocated sources, seismic multiplets, and S-wave splitting: Geophysics, **74**, no. 5, B183–B195, doi: 10.1190/1.3205028.

Dreger, D. S., and D. V. Helmberger, 1993, Determination of source parameters at regional distances with three-component sparse network data: Journal of Geophysical Research, **98**, 8107–8125, doi: 10.1029/93JB00023.

Feignier, B., and R. P. Young, 1992, Moment tensor inversion of induced microseismic events: Evidence of non-shear failures in the $-4 < M - 2$ moment magnitude range: Geophysical Research Letters, **19**, 1503–1506, doi: 10.1029/92GL01130.

Flinn, E. A., 1965, Confidence regions and error determinations for seismic event locations: Reviews of Geophysics, **3**, 1, 157–185, doi: 10.1029/RG003i001p00157.

Foulger, G. R., and S. A. Arnott, 1993, Local tomography: Volcanoes and the accretionary plate boundary in Iceland, *in* H. M. Iyer, and K. Hirahara, eds., Seismic tomography: Theory and applications: Chapman and Hall, 644–675.

Foulger, G. R., and B. R. Julian, 1993, Non-double-couple earthquakes at the Hengill-Grensdalur volcanic complex, Iceland: Are they artifacts of crustal heterogeneity?: Bulletin of the Seismological Society of America, **83**, 38–52.

Foulger, G. R., B. R. Julian, D. P. Hill, A. M. Pitt, P. Malin, and E. Shalev, 2004, Non-double-couple microearthquakes at Long Valley Caldera, California, provide evidence for hydraulic fracturing: Journal of Volcanology and Geothermal Research, **132**, 1, 45–71, doi: 10.1016/S0377-0273(03)00420-7.

Foulger, G. R., and R. E. Long, 1984, Anomalous focal mechanisms; tensile crack formation on an accreting plate boundary: Nature (London), **310**, no. 5972, 43–45.

Foulger, G. R., R. E. Long, P. Einarsson, and A. Björnsson, 1989, Implosive earthquakes at the active accretionary plate boundary in northern Iceland: Nature, **337**, no. 6208, 640–642, .

Foulger, G. R., A. D. Miller, B. R. Julian, and J. R. Evans, 1995a, Three-dimensional Vp and Vp/Vs structure of the Hengill triple junction and geothermal area, Iceland, and the repeatability of tomographic inversion: Geophysical Research Letters, **22**, 1309–1312, doi: 10.1029/94GL03387.

Foulger, G. R., A. M. Pitt, B. R. Julian, and D. P. Hill, 1995b, Three-dimensional structure of Mammoth Mtn., Long Valley caldera, from seismic tomography: EOS, Transactions of the American Geophysical Union, **76**, no. 46, F351, .

Foulger, G. R., and D. R. Toomey, 1989, Structure and evolution of the Hengill-Grensdalur volcanic complex, Iceland; Geology, geophysics, and seismic tomography: Journal of Geophysical Research, **94**, 17511–17522, doi: 10.1029/JB094iB12p17511.

Gunasekera, R. C., G. R. Foulger, and B. R. Julian, 2003, Four dimensional tomography shows progressive pore-fluid depletion at the geysers geothermal area, california: Journal of Geophysical Research, **108**, doi: 10.1029/2001JB000638.

Hanks, T. C., and H. Kanamori, 1979, A moment magnitude scale: Journal of Geophysical Research, **84**, 2348–2350, doi: 10.1029/JB084iB05p02348.

Hudson, J. A., R. G. Pearce, and R. M. Rogers, 1989, Source type plot for inversion of the moment tensor: Journal of Geophysical Research, **94**, 765–774, doi: 10.1029/JB094iB01p00765.

Jansky, J., V. Plicka, and L. Eisner, 2010, Feasibility of joint 1-D velocity model and event location inversion by the Neighbourhood algorithm: Geophysical Prospecting, **58**, 229–234, doi: 10.1111/gpr.2010.58.issue-2.

Julian, B. R., 1973, Extension of standard event location procedures: Lincoln Laboratory, MIT.

Julian, B. R., 1983, Evidence for dyke intrusion earthquake mechanisms near Long Valley caldera, California: Nature, **303**, no. 5915, 323–325, .

Julian, B. R., and D. L. Anderson, 1968, Travel times, apparent velocities and amplitudes of body waves: Bulletin of the Seismological Society of America, **58**, no. 1, 339–366, .

Julian, B. R., and G. R. Foulger, 1994, Identifying non-double-couple earthquakes by inverting seismic-wave amplitude ratios: American Geophysical Union.

Julian, B. R., and G. R. Foulger, 1996, Earthquake mechanisms from linear-programming inversion of seismic-wave amplitude ratios: Bulletin of the Seismological Society of America, **86**, 972–980.

Julian, B. R., and G. R. Foulger, 2010, Time-dependent tomography: Geophysical Journal International, **182**, 1327–1338, 10.1111/j.1365-246X.2010.04668.x.

Julian, B. R., G. R. Foulger, and F. Monastero, 2009, Seismic monitoring of EGS stimulation tests at the Coso geothermal field, California, using microearthquake locations and moment tensors: 34th Workshop on Geothermal Reservoir Engineering, Stanford University, February 9–11.

Julian, B. R., G. R. Foulger, F. C. Monastero, and S. Bjornstad, 2010a, Imaging hydraulic fractures in a geothermal reservoir: Geophysical Research Letters, **37**, L07305, 10.1029/2009GL040933.

Julian, B. R., G. R. Foulger, F. C. Monastero, and S. Bjornstad, 2010b, Imaging hydraulic fractures in a geothermal reservoir: Geophysical Research Letters, **37**, 10.1029/2009GL040933.

Julian, B. R., A. D. Miller, and G. R. Foulger, 1997, Non-double-couple earthquake mechanisms at the Hengill-Grensdalur volcanic complex, southwest Iceland: Geophysical Research Letters, **24**, 743–746, doi: 10.1029/97GL00499.

Julian, B. R., A. D. Miller, and G. R. Foulger, 1998, Non-double-couple earthquakes I. Theory: Reviews of Geophysics, **36**, 4, 525–549, doi: 10.1029/98RG00716.

Julian, B. R., A. Ross, G. R. Foulger, and J. R. Evans, 1996, Three-dimensional seismic image of a geothermal reservoir: The Geysers, California: Geophysical Research Letters, **23**, 685–688, doi: 10.1029/95GL03321.

Kanamori, H., 1977, The energy release in great earthquakes: Journal of Geophysical Research, **82**, 2981–2987, doi: 10.1029/JB082i020p02981.

Kissling, E., 1995, Velest user's guide: Institute of Geophysics, 31.

Maxwell, S., 2009, Microseismic location uncertainty: CSEG Recorder, April 41–46.

McGarr, A., 1992, Moment tensors of ten Witwatersrand mine tremors: Pure and Applied Geophysics, **139**, 781–800, doi: 10.1007/BF00879963.

Meersman, K., J.-M. Kendall, and M. van der Baan, 2009, The 1998 Valhall microseismic data set: An integrated study of relocated sources, seismic multiplets, and S-wave splitting: Geophysics, **74**, no. 5, B183–B195.

Miller, A. D., B. R. Julian, and G. R. Foulger, 1998, Three-dimensional seismic structure and moment tensors of non-double-couple earthquakes at the Hengill-Grensdalur volcanic complex, Iceland: Geophysical Journal International, **133**, 309–325, doi: 10.1046/j.1365-246X.1998.00492.x.

Press, W. H., S. A. Teukolsky, W. T. Vetterling, and B. P. Flannery, 2007, Numerical recipes — the art of scientific computing (third edition): Cambridge University Press.

Rodi, W. L., and S. C. Myers, 2008, Modeling travel-time correlations based on seismicity kernels and correlated velocity anomalies, in 2008 monitoring research review: Ground-Based Nuclear Explosion Monitoring Technologies, 475–484.

Ross, A., G. R. Foulger, and B. R. Julian, 1996, Non-double-couple earthquake mechanisms at the Geysers geothermal area, California: Geophysical Research Letters, **23**, 877–880, doi: 10.1029/96GL00590.

Ross, A., G. R. Foulger, and B. R. Julian, 1999, Source processes of industrially-induced earthquakes at the Geysers geothermal area, California: Geophysics, **64**, 1877–1889, doi: 10.1190/1.1444694.

Šílený, J., D. P. Hill, L. Eisner, and F. H. Cornet, 2009, Non-double-couple mechanisms of microearthquakes induced by hydraulic fracturing: Journal of Geophysical Research, **114**, 10.1029/2008JB005987.

Šílený, J., G. F. Panza, and P. Campus, 1992, Waveform inversion for point source moment tensor retrieval with variable hypocentral depth and structural model: Geophysical Journal International, **109**, 259–274, doi: 10.1111/gji.1992.109.issue-2.

Silver, P. G., and T. H. Jordan, 1982, Optimal estimation of scalar seismic moment: Geophysical Journal of the Royal Astronomical Society, **70**, 755–787, doi: 10.1111/gji.1982.70.issue-3.

Trifu, C.-I., D. Angus, and V. Shumila, 2000, A fast evaluation of the seismic moment tensor for induced seismicity: Bulletin of the Seismological Society of America, **90**, 1521–1527, doi: 10.1785/0120000034.

Waldhauser, F., and W. L. Ellsworth, 2000, A double-difference earthquake location algorithm: Method and application to the northern Hayward Fault, California: Bulletin of the Seismological Society of America, **90**, 1353–1368, doi: 10.1785/0120000006.

Wang, Z., M. E. Cates, and R. T. Langen, 1998, Seismic monitoring of CO_2 flooding of a carbonate reservoir: A rock physics study: Geophysics, **63**, 1604–1617, doi: 10.1190/1.1444457.

Wu, H., and J. M. Lees, 1999, Three-dimensional P and S wave velocity structures of the Coso geothermal area, California, from microseismic travel time data: Journal of Geophysical Research, **104**, 13217–13233, doi: 10.1029/1998JB900101.

Yang, X. P., , I. Bondar, and J. Bhattacharyyaet al., 2004, Validation of regional and teleseismic travel-time models by relocating ground-truth events: Bulletin of the Seismological Society of America, **94**, 897–919, doi: 10.1785/0120030148.